

# Subtropics-Related Interannual Sea Surface Temperature Variability in the Equatorial Central Pacific

Hsun-Ying Kao<sup>1</sup>, Jin-Yi Yu<sup>1\*</sup> and Tong Lee<sup>2</sup>

<sup>1</sup>. Department of Earth System Science, University of California, Irvine, Irvine, CA

<sup>2</sup>. Jet Propulsion Laboratory, California Institute of Technology, Pasadena, California

March 30, 2009

Submitted to *Journal of Climate*

---

\*. *Corresponding author address*: Dr. Jin-Yi Yu, Department of Earth System Science, University of California, Irvine, CA 92697-3100. E-mail: [jyyu@uci.edu](mailto:jyyu@uci.edu)

## Abstract

Interannual anomalies of sea surface temperature (SST) in the equatorial central Pacific are separated into a component related to the eastern Pacific SST anomalies (i.e., Type-1 SST variability) and a component not related to them (i.e., Type-2 SST variability). Lead-lagged regression and upper-ocean heat budget analysis are performed to contrast their control mechanisms. The Type-1 variability is part of canonical ENSO, which is characterized by SST anomalies extending from the eastern to central Pacific, coupled with the Southern Oscillation, and associated with distinct basin-wide subsurface evolution. This type of variability is dominated by a major 4-5 year periodicity and a minor biennial periodicity. In contrast, the Type-2 variability is dominated only by a biennial periodicity and is driven by local air-sea coupling without a basin-wide anomaly structure. In addition, Type-2 variability is associated with evident meridional connections to the subtropics in both hemispheres, particularly the Northern Hemisphere. Type-2 SST anomalies appear first in the northeastern subtropical Pacific due to surface heat flux forcing, later show up in the central equatorial Pacific through heat flux forcing and vertical advection processes, get further enhanced by zonal advection, and eventually terminate by surface heat flux. The southward spreading of trade wind anomalies within the northeastern subtropics-to-central tropics pathway of the Type-2 variability are associated with intensity variations of the subtropical high. It is also found that the Type-2 variability has become stronger since 1990, and this enhancement is related to the recent intensification of subtropical variability. This study concludes that the Type-2 interannual variability represents a tropical-subtropical interaction phenomenon that is different from conventional ENSO (i.e., Type-1 variability).

## 1. Introduction

El Niño-Southern Oscillation (ENSO) is one of the strongest variation phenomena in the climate system that dominates the interannual variability in the tropical Pacific. It is characterized by anomalous sea surface temperatures (SST) extending from the eastern to central equatorial Pacific. Prevailing ENSO theories, such as the delayed-oscillator theory (Schopf and Suarez 1988; Suarez and Schopf 1988; Battisti and Hirst 1989), have suggested that surface wind anomalies in the central Pacific induce propagating Kelvin waves to initiate ENSO events in the eastern equatorial Pacific. The Bjerknes feedback mechanism (Bjerknes 1966, 1969) then kicks in to amplify the SST anomalies and spread the anomalies westward to the central equatorial Pacific. SST variations in the central equatorial Pacific are often considered an extension of the SST anomalies from the eastern Pacific and thus part of the ENSO SST structure. A close inspection of the standard deviation of the Pacific interannual SST variability (Fig. 1), which is calculated from the  $1^\circ \times 1^\circ$  Met Office Hadley Center's Sea Ice and Sea Surface Temperature dataset (HadISST; Rayner et al. 2003), reveals that, in addition to a maximum standard deviation in the eastern Pacific, a secondary maximum appears in the central Pacific (as boxed in Fig. 1). Does this secondary maximum represent a local enhancement of the conventional ENSO SST anomalies? Or does it indicate that additional physical processes other than the conventional ENSO may also contribute to the interannual SST variability in the equatorial central Pacific?

Several recent studies suggested that variability in the central equatorial Pacific should be emphasized to better describe the interannual SST variability in the tropical Pacific. Trenberth and Stepaniak (2001) were among the first to suggest that

the zonal SST contrast between the eastern and central Pacific should be considered to capture the different evolution of El Niño events. They proposed using a Trans-Niño Index (TNI) to portray the east-west SST gradient along the equatorial Pacific. By analyzing the lead-lagged correlation between the TNI and Niño-3.4 (5°S-5°N, 170°W-120°W) SST index, they were able to better describe the ENSO propagation in the past hundred years. Larkin and Harrison (2005) also noticed that many Pacific warming events have SST anomalies concentrate near the date line without major warming in the cold tongue region. They named these events “Dateline El Niño” and suggested that these events should not be treated the same as the “conventional El Niño” because the “Dateline El Niño” events have different temperature and precipitation anomalies around the globe. They also pointed out a potential need to separate these two for seasonal forecasting purposes.

The study of Yu and Kao (2007) raised the possibility that the interannual SST variability in the central and eastern Pacific may involve different physical processes. By analyzing persistence barriers in interannual SST anomalies, they noticed that the decadal changes of the persistence barriers are different between these two regions of the equatorial Pacific. In the eastern Pacific, the persistence barriers of the Niño1+2 (10°S-0°, 80°-90°W) and Niño-3 (5°S-5°N, 90°-150°W) SST indices occurred in spring before 1976/77, shifted to summer between 1978 and 1988, and moved back to spring afterward. No such decadal changes were found for the persistence barriers of both the Niño-3.4 and Niño-4 (5°S-5°N, 160°E-150°W) SST indices. The different decadal variations lead Yu and Kao (2007) to postulate that the SST variations in the eastern and central equatorial Pacific are controlled by separate physical processes. To further examine the distinct behaviors of SST variability in these two parts of the

Pacific, Kao and Yu (2009) used a method combining both linear regression and empirical orthogonal function (EOF) analysis to separate the SST variability centered in the central equatorial Pacific from that centered in the eastern equatorial Pacific. They found different spatial patterns, evolution, periodicities, and teleconnections between these two types of SST variability. Similarly, Ashok et al. (2007) have also argued that there are ENSO-like warming events in the central Pacific, which they called “El Niño Modoki”, and these events are different from the conventional El Niño (Rasmusson and Carpenter 1982). The ENSO-like warm events are characterized by warm anomalies in the central Pacific and cold anomalies in the eastern and western Pacific.

These recent studies and the existence of a secondary maximum in equatorial SST variability indicate that there is a need to focus on examining the interannual SST variability in the central Pacific. This study aims to separate the central-Pacific SST variability into a component linked to, and a component not linked to the conventional ENSO and to identify their underlying control processes. For this purpose, lead-lagged regression and upper-ocean heat budget analyses are performed. This paper is organized as follows: The reanalysis and ocean assimilation products used in this study are described in Section 2. The ENSO-related and non-ENSO-related types of central Pacific SST variability are defined and their spatial and temporal properties are contrasted in Section 3. Heat budget analyses are presented in Section 4 to identify the controlling processes of these two types of SST variability. A further examination of the tropical-subtropical interactions for the non-ENSO-related variability is presented in Section 5. The results and their implications are summarized and discussed in Section 6.

## 2. Datasets

The major dataset used in this study is the ocean assimilation product from German Estimating the Circulation and Climate of the Ocean project (GECCO; Köhl et al. 2006), which is available through <http://www.ecco-group.org>. It is used for the analyses of subsurface ocean structures and for upper-ocean heat budget analyses and the data is available from 1952 to 2001. GECCO is produced by constraining the MIT OGCM (Ocean General Circulations Model) with various observations using an adjoint method. This method corrects the initial state and the prior (first guess) surface forcing derived from NCEP/NCAR reanalysis (Kalnay et al. 1996) to improve the fit of the OGCM to various observations. The GECCO assimilation satisfies property conservation principles, which avoids the addition of artificial sources and sinks of properties (such as heat) in obtaining the estimated state. This assimilation process makes GECCO an assimilation product suitable for ocean heat budget analyses. The dataset covers a domain from 79.5°S to 79.5°N and has a 1°×1° horizontal resolution. Vertically, it has 23 unevenly divided layers from 5 m to 5450 m. The SST standard deviation calculated from GECCO (not shown) is similar to that of Fig. 1. A secondary maximum of the standard deviation also appears in the central equatorial Pacific. In this study, interannual anomalies are obtained by removing the mean seasonal cycle from the original fields and then applying a low-pass filter to remove anomalies shorter than 12 months. For our analyses of atmospheric variables, we use the NCEP/NCAR reanalysis.

### **3. Type-1 and Type-2 SST variability in the central Pacific**

Following Chiang et al. (2004), we use a linear regression-based method to separate Pacific interannual SST variability into a conventional-ENSO component and non-conventional-ENSO component. First, we linearly regress all tropical Pacific SST anomalies with the SST anomalies averaged in an eastern Pacific box ( $5^{\circ}\text{S}$ - $5^{\circ}\text{N}$ ,  $120^{\circ}\text{W}$ - $80^{\circ}\text{W}$ ) where the maximum SST standard deviation is observed in Fig. 1. The regressed SST anomalies are considered to be the conventional-ENSO component of the variability. The residual SST anomalies obtained by removing the regressed anomalies from the original SST anomalies are considered to be the non-conventional-ENSO component of the SST variability. We then average the regressed SST anomalies in a central Pacific box ( $5^{\circ}\text{S}$ - $5^{\circ}\text{N}$ ,  $180^{\circ}$ - $140^{\circ}\text{W}$ ; as shown in Fig. 1) to obtain an index representing the strength of the conventional-ENSO SST variability in the central Pacific, which is hereafter referred to as Type-1 SST variability. Similarly, the strength of the non-conventional-ENSO SST variability in the central Pacific (i.e., Type-2 SST variability, hereafter) is represented by averaging the residual SST anomalies in the same central Pacific box. We find that the standard deviation of the Type-1 SST index is  $0.69^{\circ}\text{C}$ , while it is  $0.59^{\circ}\text{C}$  for Type-2 SST index. As expected, Type-1 is the leading type of interannual SST variability in the central Pacific, but Type-2 accounts for a nearly comparable percentage of the central Pacific variability.

We next perform lead-lagged regression analyses between the Type-1/Type-2 indices and SST anomalies in the tropical Pacific to construct the patterns and evolution of these two types of variability. The results are shown in Fig. 2. The Type-1 variability (Figs. 2a-e) shows a conventional ENSO evolution (Rasmusson and

Carpenter 1982), with SST anomalies emerging first in the cold tongue region, extending westward toward the date line, and decaying in the central Pacific. In contrast to Type-1, which has anomalies of the same sign in the central and eastern Pacific, the Type-2 variability (Fig. 2h) has a SST anomaly center in the central Pacific but weak negative anomalies in the eastern and western Pacific. Also in contrast to the Type-1 SST pattern, which is confined mostly to the equatorial region, the Type-2 SST anomaly pattern spreads over a wider latitudinal range and shows stronger associations with the subtropics (Figs. 2f-j). In addition, Type-2 SST anomalies appear in the subtropics before the onset of SST anomalies at the equator. This suggests that the subtropical Pacific plays some role in Type-2 events.

The seasonal variations of the standard deviations of these two-types of SST variability were also examined to determine their phase locking to the seasonal cycle (not shown). Both types have their weakest variability during the boreal spring, but Type-1 has its maximum standard deviation during September to November, while Type-2 has its maximum a bit later, during October to December. Therefore, we choose to measure their strength each year by averaging the indices in those months when they have their largest standard deviations. Figure 3 shows the relative strengths of these two types of variability from 1952 to 2001. The figure shows that Type-2 events can occur alone (e.g., 1979, 1991 and 1992) or together with Type-1 events (e.g., 1965, 1972, and 1975). There are also years when only Type-1 events occur (e.g., 1982, 1987 and 1997). The leading periodicities of these two types of SST variability are examined in Fig. 4 with power spectral analyses. The Type-1 index has significant power in both the 4-year and 2-year bands, which are the known leading frequencies of typical ENSO (Rasmusson and Carpenter 1982; Rasmusson et al. 1990;

Barnett 1991; Gu and Philander 1995; Jiang et al. 1995; Wang and Wang 1996). The Type-2 index is characterized by a single peak near 2-years (Fig. 4b). We will explore this biennial periodicity in more depth in Section 5.

We next examine the atmosphere and ocean structures of these two types of SST variability in Fig. 5 by calculating the lead-lagged regression between Type-1/Type-2 indices and SST, zonal wind stress and sea surface height (SSH) anomalies at the equator. The SST anomalies for Type-1 events appear first in the eastern Pacific and extend westward toward the central Pacific (Fig. 5a). In contrast, Type-2 SST anomalies are confined locally in the central Pacific with weakly out-of-phase SST anomalies in the cold tongue region (Fig. 5b). The anomalies appear to propagate eastward initially then turn westward after the event develops to larger amplitude as shown from the local maximum labeled by the asterisks in the figure. For Type-1, zonal wind stress anomalies in the western Pacific, which are essential to producing equatorial oceanic waves, show up before the onset of events (around 12 months before the peak; Fig. 5c). No such strong anomalies are found for Type-2 events (Fig. 5d). As seen in Figs. 5e and 5f, Type-1 SSH anomalies show an apparent eastward propagation across the Pacific basin, while Type-2 SSH anomalies exhibit near-local fluctuations. This lack of a basin-wide SSH anomaly propagation for Type-2 events is consistent with the absence of significant zonal wind stress anomalies in the western Pacific. To summarize, Type-1 events are characterized by basin-wide evolution of SST, zonal wind and subsurface temperature structures (as reflected in the SSH fluctuations), which are well-known features of the conventional ENSO. Type-2 events, on the other hand, are characterized by local SST, zonal wind, and subsurface

temperature structures in the central equatorial Pacific but with SST anomalies stretching into subtropics in both hemispheres.

#### 4. Upper-ocean heat budget analysis

Upper-ocean heat budget analyses are performed to identify the leading physical processes that control the evolution of the Type-1 and Type-2 SST variability. The upper-ocean temperature balance (McPhaden 2002; An and Jin 2004; Ye and Hsieh 2008) can be described by the following equation:

$$\frac{\partial T}{\partial t} = -(\bar{u} \frac{\partial T'}{\partial x} + u' \frac{\partial \bar{T}}{\partial x} + u' \frac{\partial T'}{\partial x}) - (\bar{v} \frac{\partial T'}{\partial y} + v' \frac{\partial \bar{T}}{\partial y} + v' \frac{\partial T'}{\partial y}) - (\bar{w} \frac{\partial T'}{\partial z} + w' \frac{\partial \bar{T}}{\partial z} + w' \frac{\partial T'}{\partial z}) + \frac{Q}{\rho_o C_p H} + R$$

Here,  $T$ ,  $u$ ,  $v$ ,  $w$  are, respectively, the averaged temperature, zonal, meridional and vertical current velocities in an upper ocean layer of a constant depth  $H$ . The over bars denote the climatological seasonal cycle, and the apostrophe denotes the non-seasonal anomaly from the mean. The first three groups of the terms on the right hand side of the equation represent the advection term in zonal, meridional and vertical directions, respectively. The term after the advection terms is the surface heat flux (SHF) heating term.  $Q$  is the total heat flux;  $\rho_o$  is seawater density; and  $C_p$  is the ocean heat capacity. Following Ye and Hsieh (2008), a fixed upper-ocean depth is used for the heat budget calculation. The depth is set to 50 m in the central and 20 m in the eastern equatorial Pacific, according to the climatological mixed-layer depths in these regions. The last term  $R$  denotes the residual terms, which include vertical and horizontal diffusion, as well as nonlinear terms due to the correlation of velocity and temperature gradient on

sub-monthly time scales, e.g., associated with tropical instability waves (TIWs). The latter nonlinear term is included in the residual term because only monthly averaged fields are available for the GECCO product, so sub-monthly variability cannot be evaluated explicitly. Therefore, it is important to point out that the non-seasonal anomalies in the above equation only represent anomalies with time scales longer than a month. For the sake of discussion, the interpretations of the heat budget analyses are presented for the warm phase only. Converse interpretations can be applied for the cold phase of the events.

To determine the relative importance of the various heat budget terms during the evolution of both types of SST variability, we do the lead-lagged regression of two SST indices with each heat budget term averaged over the equatorial central Pacific box and the equatorial eastern Pacific box, which are indicated in Fig. 2. Figure 6 shows the evolution of the heat budget terms over these two areas for Type-1 events. In both panels, the lag-0 corresponds to the peak time of Type-1 SST variability in the equatorial central Pacific. For this type, large budget terms appear first in the eastern Pacific box, where the initial warming tendency is contributed by the vertical advection term (green curve in Fig. 6b). This reflects the importance of thermocline fluctuation and upwelling/dowelling activities to the eastern Pacific SST anomalies. These activities are related to remote Ekman pumping in the western-central Pacific that cause equatorial Kelvin waves to propagate into the region as well as local Ekman pumping due to the variation of local trade wind. The early development of the vertical advection is consistent with the role of the Kelvin waves that often precede the mature phase of warm events in the eastern equatorial Pacific. The vertical advection term continues to play an important role throughout the

development of the SST evolution in the eastern Pacific region. After the onset of SST anomalies, both the meridional advection term (red curve in Fig. 6b) and the SHF term (black curve) pick up and become major terms in the heat budget. The former contributes a warming tendency but the latter contributes a cooling tendency, and these two terms tend to cancel each other during the evolution of the SST anomalies. The other advection term, the zonal advection (blue curve in Fig. 6b), also contributes to the SST warming but its importance is smaller than the meridional and vertical advection terms. It is noted that the amplitudes of the SHF and the zonal and meridional advection terms all increase and decrease together with the SST anomalies, indicating these terms are part of local air-sea interaction processes. Only the vertical advection term shows an apparent phase lag from the evolution of the SST anomalies in the eastern Pacific. This phase relation is consistent with the delayed-oscillator theory which suggests that thermocline variation controls the onset and termination of the ENSO SST anomalies. The heat budget results presented here are, in general, consistent with the results reported by Yu and Mechoso (2001) and Kim et al. (2007) with a coupled atmosphere-ocean GCM simulation and another assimilation product (i.e. ECCO).

In the central Pacific box (Fig. 6a), the zonal advection is the leading heat budget term for Type-1 SST evolution; this term lags the vertical advection in the eastern Pacific box by about 3 months. The meridional advection and SHF terms, again cancel each other and together have a small contribution to the development of the SST anomalies. Both the vertical advection term and the residual term are weak in this heat budget. Figures 6a and 6b indicate that Type-1 events onset with a weakening/strengthening of the vertical advection over the cold tongue region and

then expand into the central Pacific by zonal advection. In other words, the Type-1 SST variability in the central Pacific is produced by the zonal advection related to the thermocline-controlled SST anomalies from the eastern Pacific.

Figure 7 shows the evolution of the regressed heat budget terms for the Type-2 variability in the eastern and central equatorial boxes. In both panels, the lag-0 corresponds to the time when the Type-2 SST variability peaks in the central equatorial Pacific. In contrast to Type-1, there are no large heat budget terms in the eastern Pacific box (Fig. 7b), except the SHF term (black curve). We find that most of the SHF term is contributed by the shortwave radiation and the latent heat flux. It is likely that the heating effect caused by the shortwave radiation is overestimated here, because our budget calculation does not consider solar penetration and deposits all the solar flux in the budget layer. The heat budget terms evolve mainly in the central Pacific box (Fig. 7a), suggesting that Type-2 events are not resulted from the westward spreading of interannual SST variability from the eastern equatorial Pacific. Figure 7a shows that the initial warming of Type-2 events is contributed mostly by the SHF term (black curve) and the vertical advection term (green curve). During the developing stage, the zonal and meridional advection term (blue and red curves) strengthen and the zonal advection term becomes the leading contributor to the growth of temperature anomalies. It is important to note that both the meridional and vertical advection terms never change phase during the evolution, while the zonal advection term reverses its sign a couple of months after the peak of the events. These different phase relations suggest that the meridional and vertical advection terms are not involved in the termination/decay of Type-2 events, but the zonal advection term is. The latter process is associated with the anomalous westward advection of cold-

tongue water towards the central equatorial Pacific during the termination of a warm event and the initiation of a cold event. In fact, we find that all the linear advection terms for the Type-2 are dominated by the advection of mean temperature gradients by anomalous currents (not shown). This finding suggests that surface wind variations, which induce the surface current anomalies, are important to the evolution of the Type-2 SST variability. Figure 7 also shows that the SHF and the residual terms are the other participating in the termination of the Type-2 SST variability.

As noted in Fig. 2, Type-2 SST anomalies show up first in the northeastern subtropical Pacific and then extend southwestward toward the central equatorial Pacific. To understand how the anomalies spread equatorward, we examine the regressed heat budget terms along a meridional sector that links the local Type-2 SST anomaly centers from 12°S to 18°N. The black lines in Fig. 2h denote this meridional sector. Figure 8 shows the meridional evolution of the tendency of upper ocean temperature and each heat budget term. The abscissa shows the lagged months from 18 months before to 18 months after the peak of the Type-2 variability. The temperature tendency term shows that Type-2 events begin to warm the northern subtropics around 10°-15°N, about 6 months before the warming shows up at the equator (Fig. 8a). The warming gradually spreads southward and reaches the equator around lag -12 months. The warming at the equator increases and then extends further to the Southern Hemisphere. The heat budget analysis indicates that the SHF term is responsible for the initial warming in the northern subtropics and the later warming at the equator (Fig. 8b). The vertical advection (Fig. 8d) is the leading advection term that helps the onset of the equatorial warming. A few months later, the zonal advection dominates the warming at the equator (Fig. 8c). During the decaying stage

(lags 3-15 months), the SHF term (Fig. 8a), the zonal advection term (Fig. 8c), and the residual term (Fig. 8f) together contribute to the termination of upper ocean temperature anomalies at the equator. The warming caused by the meridional advection is not located exactly at the equator but a little to the north and south. The meridional advection also causes a weak cooling right at the equator. As a result, the area-averaged meridional advection has a net contribution to the initial warming in the equatorial region. As mentioned earlier, the Type-2 variability is dominated by the advection of climatological temperature gradient by anomalous currents. The larger warming effect of the meridional advection off the equator is consistent with the larger meridional temperature gradient of the climatological temperature gradient off than at the equator. The meridional advection term is also responsible for the extension of the warming into the Southern Hemisphere, as indicated by Fig. 8e.

Note that the meridional advection by the Ekman currents and the vertical advection due to local Ekman pumping that impact the central-Pacific SST may both be associated with the strength variations of shallow meridional overturning circulations, often referred to as the subtropical cell or STC (after McCreary and Lu 1994). The subsurface branch of the STC (the equatorward pycnocline flow) has an interior pathway that connects the central-equatorial Pacific with the off-equatorial and subtropical regions (e.g., Fig. 2 of Lee and Fukumori 2003). The variation of the trade winds could cause an oscillation of the STC, which involves variations in the poleward Ekman current at the surface, the equatorward pycnocline flow, and the upwelling that connects the two. It is conceivable that the oscillation of the STC in response to trade wind variations would affect the meridional and vertical advective tendencies of the upper-ocean temperature in the central-equatorial Pacific. The

specific relation between the Type-2 SST variability in the equatorial central Pacific and the interannual variation of STC deserves further studies but is beyond the scope of this study.

To further examine the validity of the regression results presented in Fig. 8, we perform a case study with the 1990/91 warming event, which is a pure Type-2 event as indicated in Fig. 3. Figure 9 shows the evolution of SST anomalies from May 1990 to February 1991. It shows that positive SST anomalies in this event appeared first in the northeastern subtropics in May 1990 (Fig. 9a), gradually extended to the central equatorial Pacific (Fig. 9b), and formed a SST anomaly pattern linking the northeastern subtropics to the central tropical regions after August 1990 (Fig. 9c). As the event developed into its peak phase in February 1991 (Fig. 9d), a rotated V-shape SST anomaly pattern was established in the central equatorial Pacific that extended eastward and poleward into the both hemispheres. The upper-ocean heat budget analyses for this event along the same meridional sector of Fig. 8 are shown in Fig. 10. The figure indicates that the SHF term initiates the warming around  $10^{\circ}$  to  $15^{\circ}\text{N}$  at the beginning of the event (Fig. 10a) - consistent with Fig. 8b. Similar to the regressed budget analysis shown in Fig. 8, both the zonal advection term (Fig. 10b) and vertical advection term (Fig. 10d) contribute to the development of the event (August 1990 - February 1991). A little different from the regressed budget, the meridional advection term begins earlier and contributes to the early development of this particular event. But in general, the pattern and evolution of the meridional advection term are consistent with those revealed by the regressed analysis. It is interesting to notice that, consistent with Fig. 8e, the meridional term tends to have maximum north or south off equator (Fig. 10d). The upper-ocean heat budget of the 1990-91 Type-2 event is, in

general, consistent with that revealed by the regressed heat budget analysis, although discrepancies exist. Both the case and regressed studies suggest that the Type-2 SST variability in the equatorial central Pacific originates from the subtropics and evolves through the aforementioned surface heat flux forcing and ocean advection processes.

## **5. Tropical and Subtropical Linkages for Type-2 Events**

In this section, we look further into the subtropical-tropical interaction associated with the Type-2 SST variability. In these regions, the surface current is related to the evolution of surface wind stress. Figure 11 shows the evolution of zonal wind stress, meridional wind stress, and sea level pressure (SLP) anomalies along the meridional sector where we examine the upper ocean heat budget. During the initial northeastern subtropical warming, surface westerly and southerly anomalies appear in the subtropics (Fig. 11a-b), which weaken the climatologic northeasterly trade winds, reduce surface evaporation, and produce positive SST anomalies. The positive SST anomalies intensify negative SLP anomalies and extend the surface wind anomalies southward toward the equator, as shown in the figure between lag  $-12$  and lag  $-6$  months. As the surface wind stress anomalies arrive at the equator, the reduced trade winds weaken the upwelling of cold subsurface ocean water and reduce the northward advection of warm SSTs through Ekman transport. As a result, a warming starts at the equator (recall Figs. 8d-e). At the same time, the positive zonal wind stress anomalies induce eastward current anomalies, which facilitate the intrusion of the warmer western-Pacific waters and causes warming in the equatorial central Pacific. Figure 11 shows that, as the Type-2 SST anomalies develop in the equatorial central Pacific, SLP anomalies in the both hemispheres deepen and spread both the zonal and

meridional wind anomalies equatorward. The equatorward spread is particularly obvious for the zonal wind stress anomalies in the Southern Hemisphere. As the zonal wind stress establish to the south of the equator, the wind-induced meridional Ekman transport is particularly important to develop the Type-2 SST variability into the Southern Hemisphere (as seen in Fig. 8e).

The above analyses indicate that SLP variations control surface wind anomalies and are important to the Type-2 SST variability. In Fig. 12, we contrast the associated SLP anomaly patterns between the Type-1 and Type-2 SST variability. The values shown in the figure are the correlation coefficients between SLP anomalies (from the NCEP/NCAR reanalysis) and the Type-1/Type-2 SST indices. Figure 12a shows that Type-1 SST variability is, as expected, associated with the Southern Oscillation pattern, which is characterized by out-of-phase SLP anomalies between the eastern and western tropical Pacific. The SLP variations over the Maritime Continent region are linked to SLP over the eastern equatorial Pacific through the Walker Circulation. Figure 12b shows that the SLP anomaly pattern associated with the Type-2 variability does not resemble the Southern Oscillation. Instead, the SLP variations over the Maritime Continent are linked to the SLP variations in the subtropics of both the Northern and Southern Pacific, suggesting that the connection through meridional circulation may be more important here. We notice that the center of the subtropical SLP anomalies in the Northern Hemisphere is located at the southern boundary of the mean wintertime subtropical sea-level high (not shown). Therefore, the SLP anomalies shown in Fig. 12b represent variations in the extension and the strength of the northern subtropical high. We find that the power spectrum of a subtropical high index, which is defined as the SLP anomalies averaged

in the northeastern subtropics ( $20^{\circ}\text{N}$ - $40^{\circ}\text{N}$  and  $160^{\circ}\text{W}$ - $110^{\circ}\text{W}$ ), also shows a significant peak near the 2-year band (Fig. 13). This peak is consistent with the dominant periodicity found for the Type-2 SST index (see Fig. 4b). This is a further evidence suggesting the existence of a close linkage between the northeastern subtropical and the central equatorial Pacific on interannual timescales.

The results presented so far indicate that the subtropical forcing plays an important role in producing the Type-2 SST variability, and that this type of variability is as important as the Type-1 SST variability in generating the interannual warm and cold events in the tropical Pacific. We also notice that the Type-2 SST variability has experienced decadal/interdecadal variations. Figure 14 shows the variations of SST standard deviation along the northeastern subtropical-to-equatorial central Pacific pathway (i.e., the black lines shown in Fig. 2h) from 1952 to 2001 using a 10-year running window. It shows that the SST variability in the northern subtropics is stronger in the 1960s and 1990s but weaker in the 1970-80s. This decadal variation of subtropics SST is in accordance with the Type-2 events identified in Fig. 3, which shows that Type-2 events have been more intense and more frequent since the 1990s. This result suggests that there is a decadal/interdecadal variability in the subtropics SST variability and this subtropical forcing to the equatorial central Pacific and the Type-2 SST variability has become more active since 1990.

## **6. Conclusions and Discussion**

In this study, we focused on analyzing interannual SST variability in the equatorial central Pacific and separating the anomalies into a Type-1 variability that is

related to the equatorial eastern Pacific and a Type-2 variability that is not. The Type-1 variability is part of the conventional ENSO that emerges in the eastern Pacific. In contrast, the Type-2 variability is found to have a strong connection to the subtropical Pacific. Heat budget analyses were performed to identify the leading physical processes for these two types of SST variability. The results show that, as expected, the Type-1 SST variability in the central Pacific results from the zonal advection of the thermocline-controlled SST variations from the eastern equatorial Pacific. As for the Type-2 variability, it is linked to the northeastern subtropics through surface wind forcing and associated surface ocean advections. This study suggests that there is a distinct interannual SST variability in the equatorial central Pacific that is not a component of the conventional ENSO events but is closely related to subtropical influences and forcing, and that the Type-2 SST variability may have been stronger since the 1990.

The Type-2 SST variability identified in this study resembles the Northern Hemispheric part of the so-called meridional mode of the tropical Pacific atmosphere-ocean variability (Chiang and Vimont 2004), which also exhibits a SST anomaly pattern extending from the eastern part of the northern subtropics to the equatorial central Pacific. Vimont et al. (2001) suggested a seasonal footprint mechanism to explain how mid-latitude atmospheric variability might affect tropical SST variability via the atmosphere-ocean coupling in the subtropics. Our current study sustains the suggestion from these earlier studies that a significant part of the SST variability in the equatorial Pacific is related to the subtropical forcing. Our upper-ocean budget analyses further identify the specific physical processes that bring the subtropical influences into the tropical Pacific. In this regard, our study is consistent with these

studies of the Pacific meridional mode. However, the meridional mode was emphasized as a precursor for the onset of conventional ENSO events (e.g., Chang et al. 2007), because meridional mode events tend to produce westerly wind anomalies in the western Pacific and then induce the oceanic waves that develop ENSO events. Our study, on the other hand, emphasizes that the subtropics-related Type-2 SST variability in the central Pacific should be viewed as an interannual SST variability distinct from conventional ENSO events. Through the heat flux and upper ocean processes, Type-2 warm/cold events may occur in the years with or without ENSO activities. Different flavors of ENSO events, such as the convectonal El Niño and dateline El Niño, may be explained as the alternation of the tropical coupled Type-1 SST variability and the subtropics-forced Type-2 SST variability.

The origin of the interannual variability in the subtropical high is beyond the scope of this study. Nevertheless, we want to point out that, in addition to considering it a result of winter atmospheric transient variability (Vimont et al. 2001), another possible source is the influence from the Indian and Asian-Australian monsoons, which also exhibit a strong quasi-biennial periodicity (Meehl and Arblaster 2001, 2002). We find that the correlation between the Indian monsoon circulation index of Webster and Yang (1992) is 0.55 with our subtropical high index and 0.46 with our Type-2 SST index. The relatively high correlations imply the possibility of close relations among these three climate phenomena on the biennial timescales. The recent modeling study of Yu et al. (2009) showed that by reducing biennial variability in the Indian and Australian monsoons in a numerical experiment with the NCAR Community Climate System Model 3.0, the biennial SST variability produced by that model in the central equatorial Pacific is also diminished. Further studies on the role

of the subtropics-related Type-2 variability in the establishment of biennial variability in the tropics are clearly warranted.

***Acknowledgments.*** This research was support by NASA (NNX06AF49H) and JPL (subcontract No.1290687). Data analyses were performed at University of California, Irvine's Earth System Modeling Facility.

## References

An, S.-I., and F.-F. Jin, 2004: Nonlinearity and asymmetry of ENSO. *J. Climate*, **17**, 2399–2412.

Ashok K., S. Behera, S. A. Rao, H. Weng, T. Yamagata, 2007: El Niño Modoki and its possible teleconnection. *J. Geophys Res.*, **112**, C11007, doi:10.1029/2006JC003798.

Barnett, 1991: The interaction of multiple time scales in the tropical climate system. *J. Climate*, **4**, 269–285.

Battisti, D. S. and A. C. Hirst, 1989: Interannual variability in the tropical atmosphere-ocean system: Influence of the basic state, ocean geometry, and nonlinearity. *J. Atmos. Sci.*, **46**, 1687-1712.

Bjerknes J., 1966: A possible response of the atmospheric Hadley circulation to equatorial anomalies of ocean temperature. *Tellus*, **18**, 820–829.

Bjerknes, J., 1969: Atmospheric teleconnections from the equatorial Pacific. *Mon. Wea. Rev.*, **97**, 163–172.

Chang P., L. Zhang, R. Saravanan, D. J. Vimont, J. C. H. Chiang, L. Ji, H. Seidel, M. K. Tippett, 2007: Pacific meridional mode and El Niño—Southern Oscillation, *Geophys. Res. Lett.*, **34**, L16608, doi:10.1029/2007GL030302.

Chiang, J.C.H., and D.J. Vimont, 2004: Analogous Pacific and Atlantic meridional modes of tropical atmosphere–ocean variability. *J. Climate*, **17**, 4143–4158.

Gu, D., and S. G. H. Philander, 1995: Secular changes of annual and interannual variability in the Tropics during the past century. *J. Climate*, **8**, 864–876.

Jiang, N., J. D. Neelin, and M. Ghil, 1995: Quasi-quadrennial and quasi-biennial variability in the equatorial Pacific. *Climate Dyn.*, **12**, 101–112.

Kalnay, E., M. Kanamitsu, R. Kistler, W. Collins, D. Deaven, L. Gandin, M. Iredell, S. Saha, G. White, J. Woollen, Y. Zhu, A. Leetmaa, R. Reynolds, M. Chelliah, W. Ebisuzaki, W. Higgins, J. Janowiak, K. Mo, C. Ropelewski, J. Wang, R. Jenne, and D. Joseph, 1996: The NCEP/NCAR 40-year reanalysis project. *Bull. Amer. Meteor. Soc.*, **77**, 437–471.

Kao H.-Y., and J.-Y. Yu, 2009: Contrasting eastern-Pacific and central-Pacific types of ENSO. *Journal of Climate*, **22**, 615–632.

Kim, S.B., T. Lee, and I. Fukumori, 2007: Mechanisms Controlling the Interannual Variation of Mixed Layer Temperature Averaged over the Niño-3 Region. *J. Climate*, **20**, 3822–3843.

Köhl, A., D. Dommenges, K. Ueyoshi, and D. Stammer, 2006: The Global ECCO 1952 to 2001 Ocean Synthesis. Technical Report 40, see also <http://www.ecco-group.org/ecco1/reports.html>.

Larkin, N. K., and D. E. Harrison, 2005: Global seasonal temperature and precipitation anomalies during El Niño autumn and winter, *Geophys. Res. Lett.*, **32**, L16705, doi:10.1029/2005GL022860.

Lee, T., and I. Fukumori, 2003: Interannual to decadal variation of tropical-subtropical exchange in the Pacific Ocean: boundary versus interior pycnocline transports. *J. Climate*. **16**, 4022-4042.

McCreary, J. P., and P. Lu, 1994: Interaction between the subtropical and equatorial ocean circulations: The subtropical cell. *J. Phys. Oceanogr.*, **24**, 466–497.

McPhaden, M.J., 2002: Mixed Layer Temperature Balance on Intraseasonal Timescales in the Equatorial Pacific Ocean. *J. Climate*, **15**, 2632–2647.

Meehl, G.A., J.M. Arblaster, 2001: The Tropospheric Biennial Oscillation and Indian Monsoon Rainfall. *Geophys. Res. Lett.*, **28**, 1731-1734.

Meehl, G.A., J.M. Arblaster, 2002: The Tropospheric Biennial Oscillation and Asian-Australian Monsoon Rainfall. *J. Climate*, **15**, 722-744.

Rasmusson, E. M. and T. H. Carpenter, 1982: Variations in tropical sea-surface temperature and surface wind fields associated with the Southern Oscillation El-Niño. *Mon. Wea. Rev.*, **110**, 354-384.

Rasmusson, E. M., X. Wang, and C. F. Ropelewski, 1990: The biennial component of ENSO variability. *J. Mar. Syst.*, **1**, 71–90.

Rayner, N.A., D.E. Parker, E.B. Horton, C. K. Folland, L. V. Alexander, D. P. Rowell, E.C. Kent, and A. Kaplan, 2003: Global analyses of sea surface temperature, sea ice, and night marine air temperature since the late nineteenth century. *J. Geophys. Res.*, **108**, 4407.

Schopf, P.S., and M.J. Suarez, 1988: Vacillations in a Coupled Ocean–Atmosphere Model. *J. Atmos. Sci.*, **45**, 549–566.

Suarez, M. J. and P. S. Schopf, P. S., 1988: A delayed action oscillator for ENSO. *J. Atmos. Sci.*, **45**, 3283-3287.

Trenberth, K. E., D. P. Stepaniak, 2001: Indices of El Niño evolution. *J. Climate*, **14**, 1697-1701.

Vimont, D., D. Battisti, and A. Hirst, 2001: Footprinting: A Seasonal Connection Between the Tropics and Mid-Latitudes, *Geophys. Res. Lett.*, **28**(20), 3923-3926.

Wang B., and Y. Wang, 1996: Temporal Structure of the Southern Oscillation as Revealed by a Waveform and a Wavelet Transform. *J. Climate*, **9**, 1586-1598

Webster, P. J. and S. Yang, 1992: Monsoon and ENSO: Selectively Interactive Systems. *Quart. J. Roy. Meteor. Soc.*, **118**, 877-926.

Ye, Z., and W.W. Hsieh, 2008: Changes in ENSO and Associated Overturning Circulations from Enhanced Greenhouse Gases by the End of the Twentieth Century. *J. Climate*, **21**, 5745–5763.

Yu, J.-Y. and C.R. Mechoso, 2001: A coupled atmosphere-ocean GCM study of the ENSO cycle. *Journal of Climate*, **14**, 2329-2350.

Yu, J.-Y., and H.-K. Kao, 2007: Decadal changes of ENSO persistence barrier in SST and ocean heat content indices 1958-2001. *J. Geophys. Res.*, **112**, D13106, doi:10.1029/2006JD007654.

Yu, J.-Y., F. Sun, and H.-Y. Kao, 2009: Contributions of Indian Ocean and Monsoon Biases to the Excessive Biennial ENSO in CCSM3. *Journal of Climate*, **22**, 1850-1958.

## Figure Caption

Figure 1. Standard deviation of the interannual SST anomalies in the tropical Pacific calculated from the  $1^\circ \times 1^\circ$  Met Office Hadley Center's Sea Ice and Sea Surface Temperature dataset (HadISST). The standard deviation is calculated during the half year October-through-March when ENSO events typically reach their mature stage. The box denotes the central Pacific region, where the second maximum variability is located. The contour interval is  $0.2^\circ\text{C}$ .

Figure 2. Lead-lagged regression coefficients between SST anomalies in the tropical Pacific and the Type-1 (panels a-e) and Type-2 SST indices (panels f-j). Contour intervals are  $0.2^\circ\text{C}/\text{month} \times ^\circ\text{C}$ . The values in the parenthesis at the upper left of the panels indicate the lag months and the boxes denote areas in the central and eastern Pacific used to define Type-1 and Type-2 indices. The black lines in (h) connect local maximum variability centers from  $12^\circ\text{S}$  to  $18^\circ\text{N}$ .

Figure 3. Yearly variability of Type-1 (blue) and Type-2 (red) SST indices from 1952 to 2001. The ordinate is the indices in  $^\circ\text{C}$ .

Figure 4. Power spectra of the (a) Type-1 and (b) Type-2 SST indices. The solid and the dashed curves denote the 99% and 95% significant levels, respectively.

Figure 5. Lead-lagged regression of SST (a-b), zonal wind stress (c-d) and SSH (e-f) anomalies at the equator with Type-1 (left panels) and Type-2 SST indices (right panels). The contour intervals are  $0.2 \text{ }^\circ\text{C}/\text{month} \times ^\circ\text{C}$ ,  $0.2 \text{ m/s} \times \text{month} \times ^\circ\text{C}$ , and 1

cm/month\*°C, respectively. The abscissa is the longitude and the ordinate shows time lags in months. The asterisks in (a, b) indicate the local maximum.

Figure 6. Lead-lagged regression of Type-1 index with heat budget terms in the (a) central Pacific and (b) eastern Pacific. The black, blue, red, green and magenta lines denote the surface heat flux (SHF), zonal, meridional, vertical advection and residual terms, respectively. The light shaded area shows the 95% confidence interval for each term.

Figure 7. Same as Fig. 6, but regression with Type-2 SST index.

Figure 8. Meridional evolution of regressed heat budget terms for Type-2 SST events along the black lines in Fig. 2h: (a) SST tendency (b) surface heat flux (SHF) (c)  $-udT/dx$  (d)  $-wdT/dz$  (e)  $-vdT/dy$  and (f) residual. Contour intervals are 0.02 °C/month\*°C.

Figure 9. Evolution of SST anomalies in the tropical Pacific from May 1990 to February 1991. The contour intervals are 0.5°C. The “year/month” are indicated in the bottom-left of the panels.

Figure 10. Meridional evolutions of the heat budget terms along the black lines in Fig. 2h for the 1990 event: (a) surface heat flux (SHF) (b)  $-udT/dx$  (c)  $-wdT/dz$  and (d)  $-vdT/dy$ . The evolutions are shown for the period from May 1990 to May 1991. Contour intervals are 0.02 °C.

Figure 11. Meridional evolution of Type-2 (a) zonal wind stress (b) meridional wind stress and (c) SLP along the black lines in Fig. 2h. Contour intervals are 0.2 cm/s\*month\*°C for wind stress and 0.2 mb/month\*°C for SLP.

Figure 12. Correlation coefficients of sea level pressure with (a) Type-1 and (b) Type-2 SST indices. The contour interval is 0.1.

Figure 13. Power spectrum of subtropical high variability calculated from the sea level pressure anomalies averaged in an area between 20°N-40°N and 160°W-110°W. The thin-line denotes the 95% significance level and the dashed-line denotes the red-noise spectrum.

Figure 14. The standard deviations of SST anomalies along the black lines in Fig. 2h from 1958 to 2001 calculated with a 10-year running window. Contour interval is 0.2 °C. The abscissa shows the years.

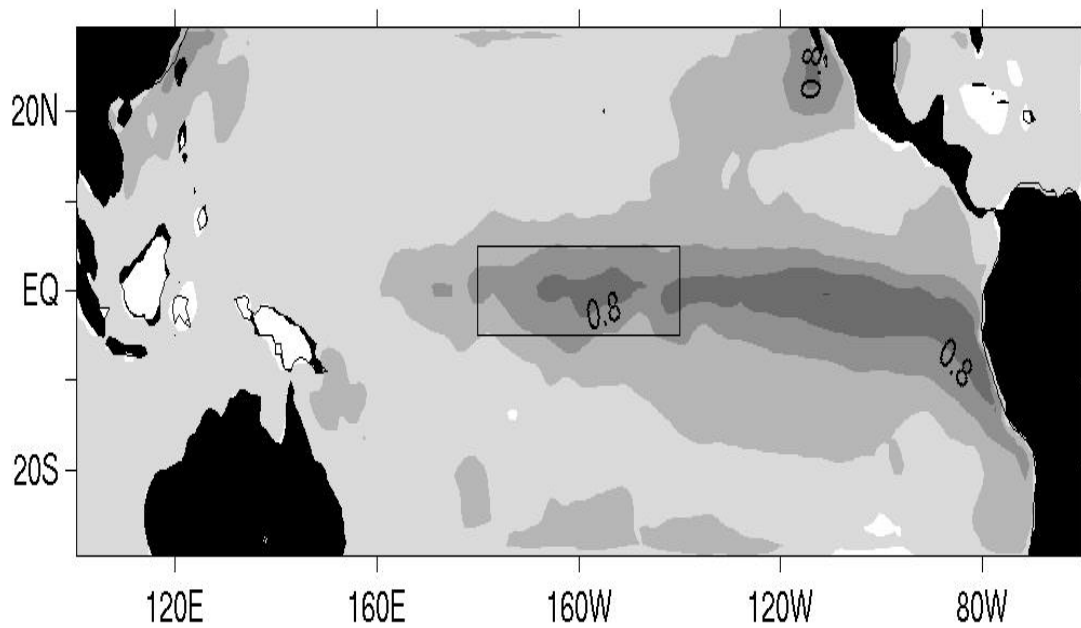


Figure 1. Standard deviation of the interannual SST anomalies in the tropical Pacific calculated from the  $1^{\circ}\times 1^{\circ}$  Met Office Hadley Center's Sea Ice and Sea Surface Temperature dataset (HadISST). The standard deviation is calculated during the half year October-through-March when ENSO events typically reach their mature stage. The box denotes the central Pacific region, where the second maximum variability is located. The contour interval is  $0.2^{\circ}\text{C}$ .

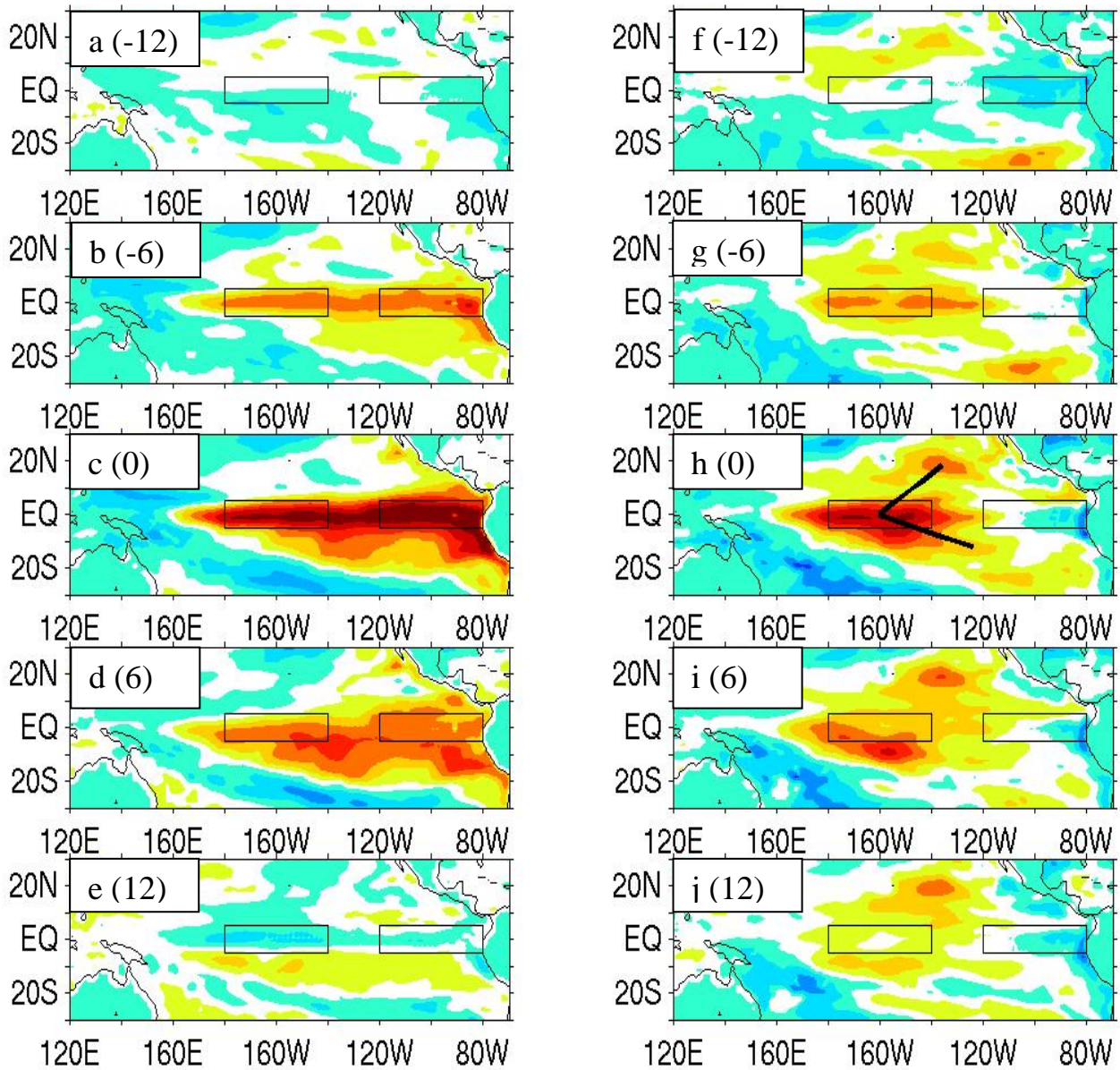


Figure 2. Lead-lagged regression coefficients between SST anomalies in the tropical Pacific and the Type-1 (panels a-e) and Type-2 SST indices (panels f-j). Contour intervals are  $0.2^{\circ}\text{C}/\text{month}^{\circ}\text{C}$ . The values in the parenthesis at the upper left of the panels indicate the lag months and the boxes denote areas in the central and eastern Pacific used to define Type-1 and Type-2 indices. The black lines in (h) connect local maximum variability centers from  $12^{\circ}\text{S}$  to  $18^{\circ}\text{N}$ .

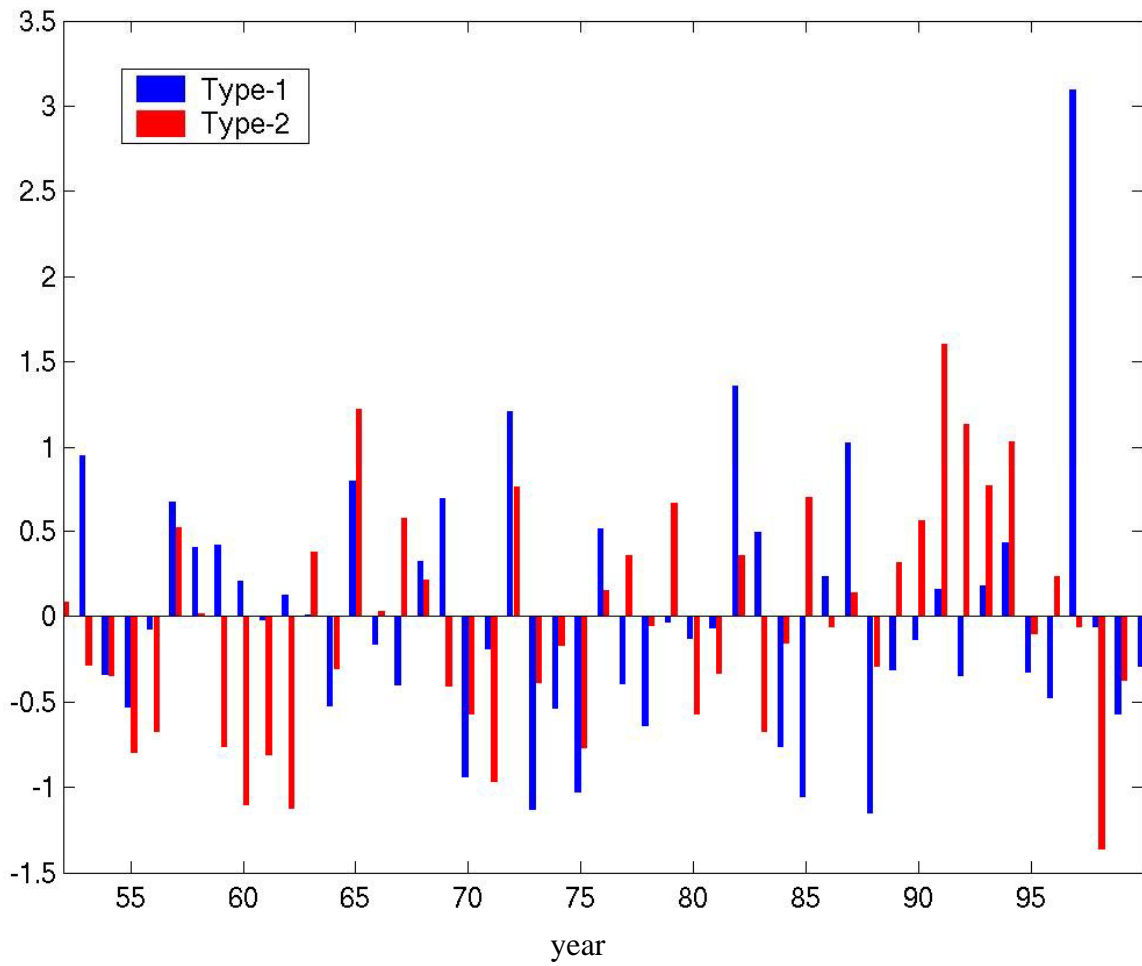


Figure 3. Yearly variability of Type-1 (blue) and Type-2 (red) SST indices from 1952 to 2001. The ordinate is the indices in °C.

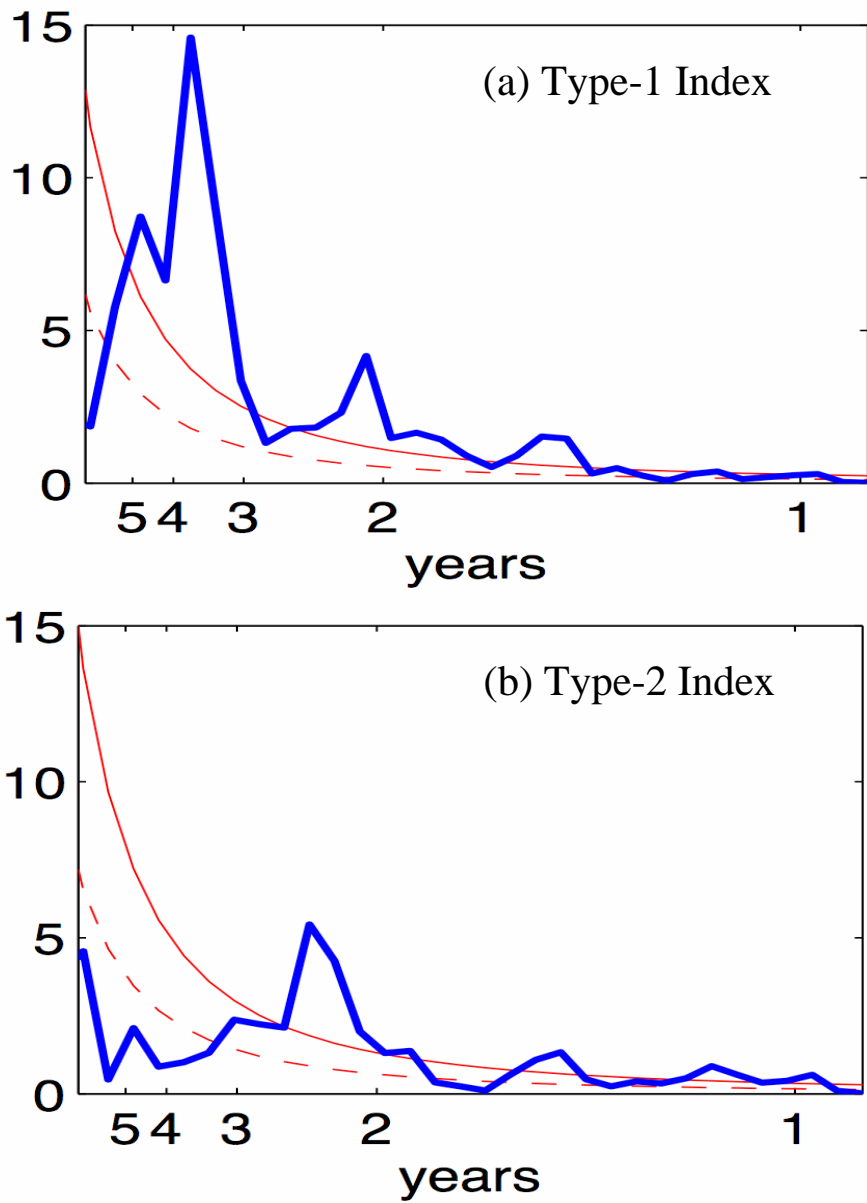


Figure 4. Power spectra of the (a) Type-1 and (b) Type-2 SST indices. The solid and the dashed curves denote the 99% and 95% significant levels, respectively.

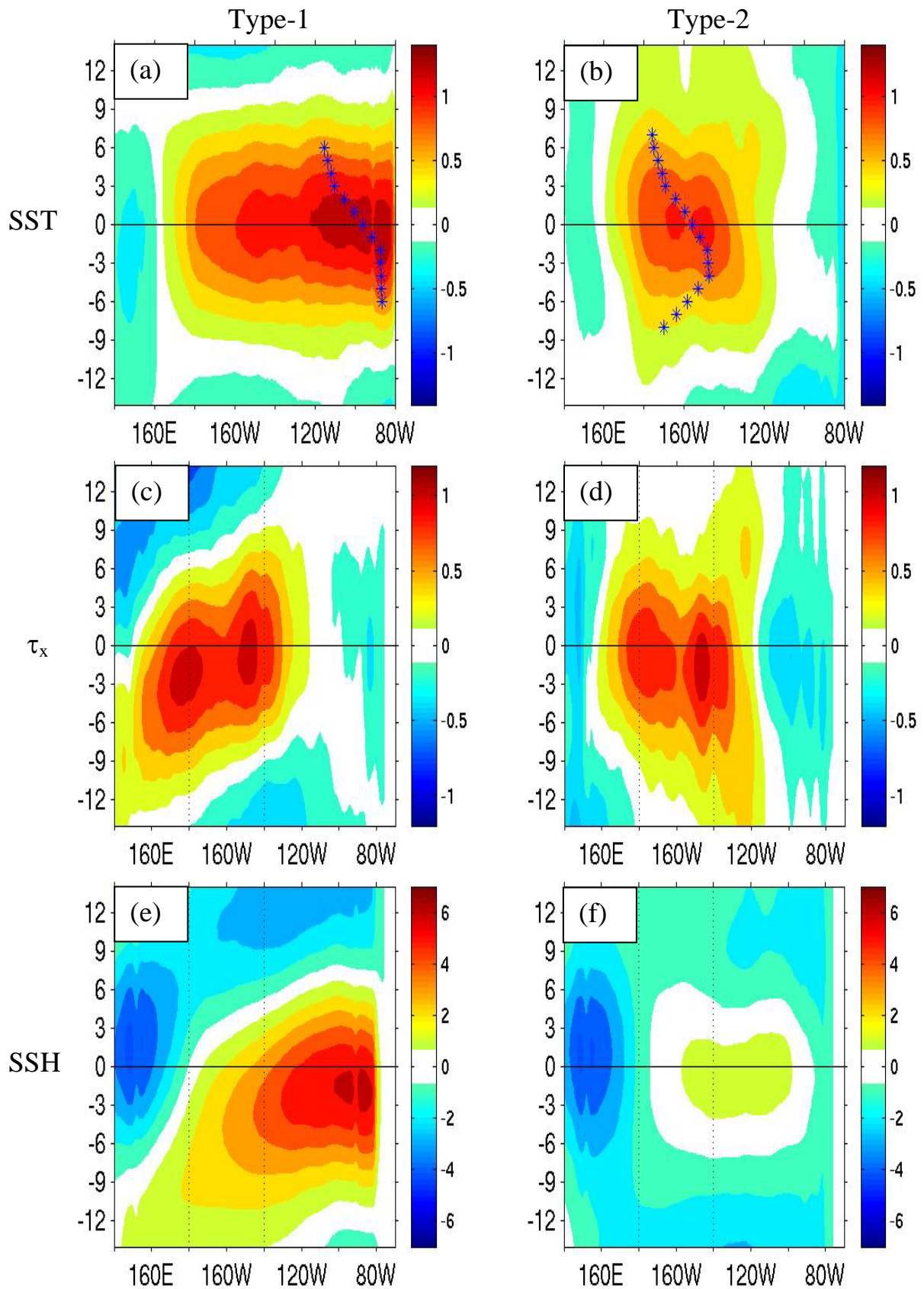


Figure 5. Lead-lagged regression of SST (a-b), zonal wind stress (c-d) and SSH (e-f) anomalies at the equator with Type-1 (left panels) and Type-2 SST indices (right panels). The contour intervals are  $0.2 \text{ } ^\circ\text{C}/\text{month} \cdot ^\circ\text{C}$ ,  $0.2 \text{ m/s} \cdot \text{month} \cdot ^\circ\text{C}$ , and  $1 \text{ cm}/\text{month} \cdot ^\circ\text{C}$ , respectively. The abscissa is the longitude and the ordinate shows time lags in months. The asterisks in (a, b) indicate the local maximum.

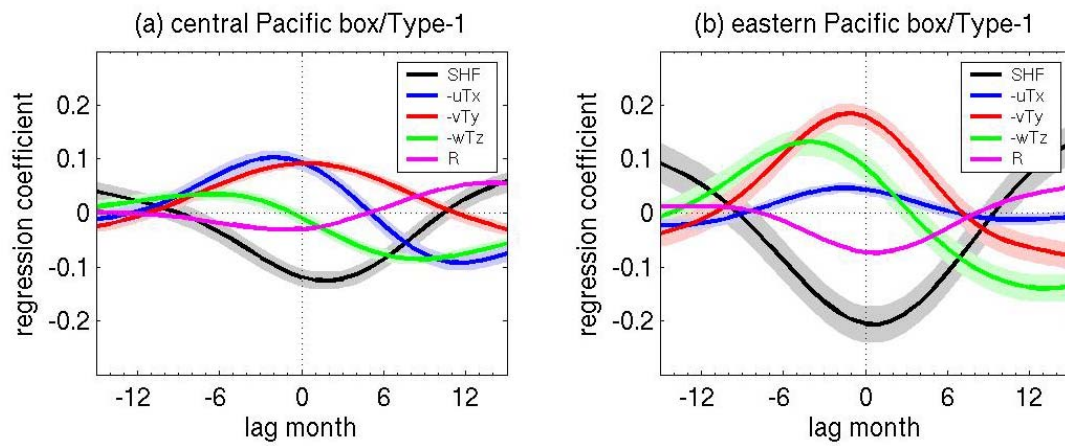


Figure 6. Lead-lagged regression of Type-1 index with heat budget terms in the (a) central Pacific and (b) eastern Pacific. The black, blue, red, green and magenta lines denote the surface heat flux (SHF), zonal, meridional, vertical advection and residual terms, respectively. The light shaded area shows the 95% confidence interval for each term.

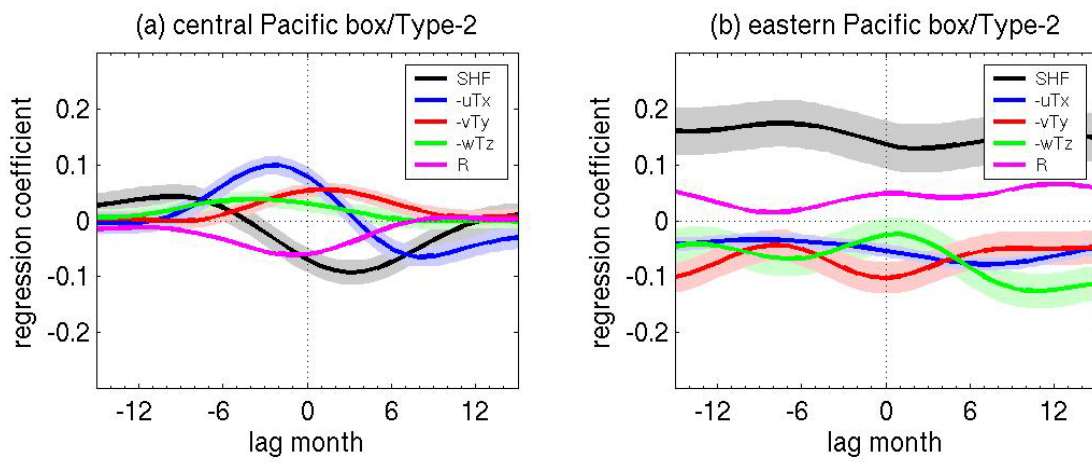


Figure 7. Same as Fig. 6, but regression with Type-2 SST index.

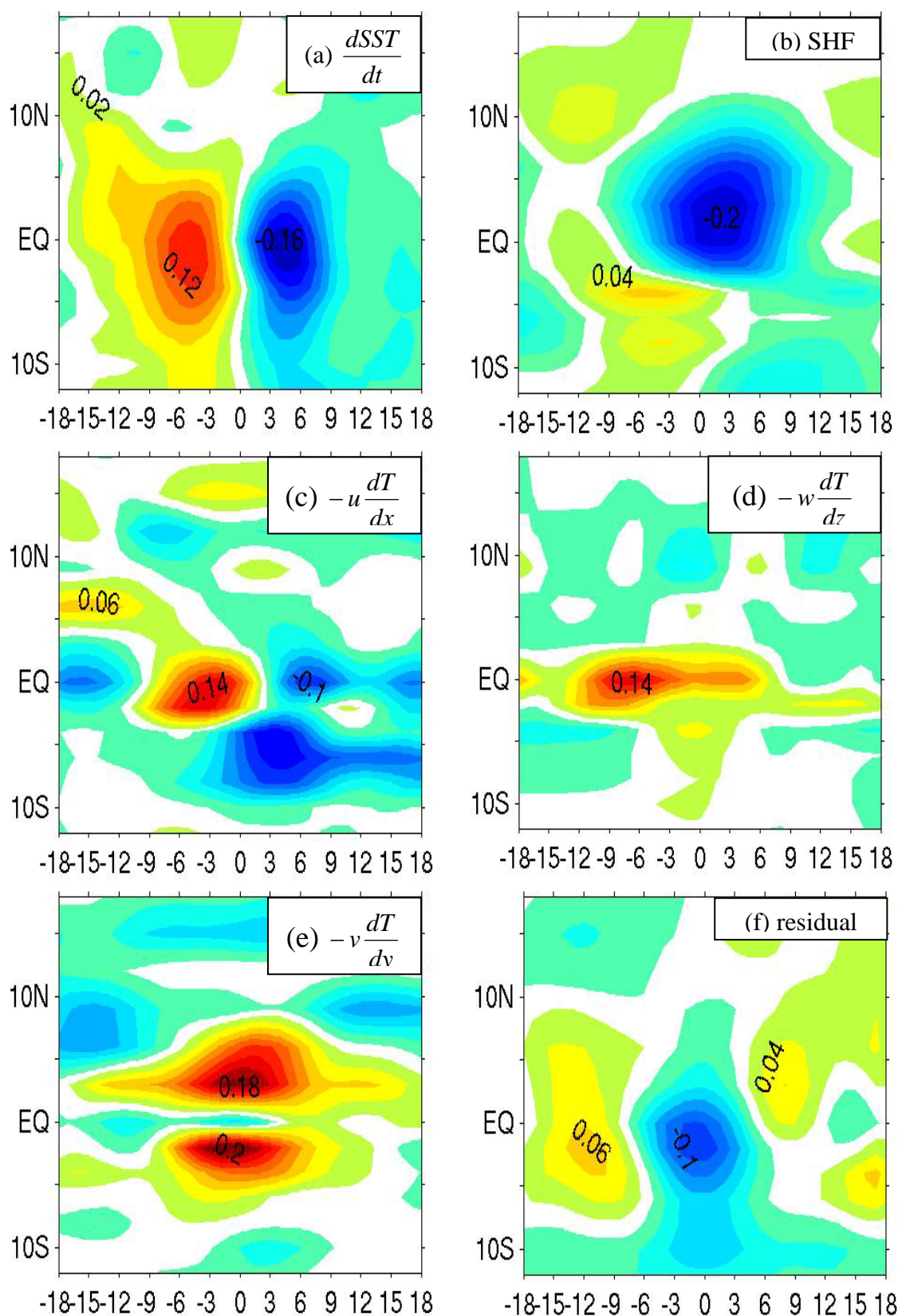


Figure 8. Meridional evolution of regressed heat budget terms for Type-2 SST events along the black lines in Fig. 2h: (a) SST tendency (b) surface heat flux (SHF) (c)  $-u \frac{dT}{dx}$  (d)  $-w \frac{dT}{dz}$  (e)  $-v \frac{dT}{dy}$  and (f) residual. Contour intervals are  $0.02 \text{ } ^\circ\text{C}/\text{month} \cdot ^\circ\text{C}$ .

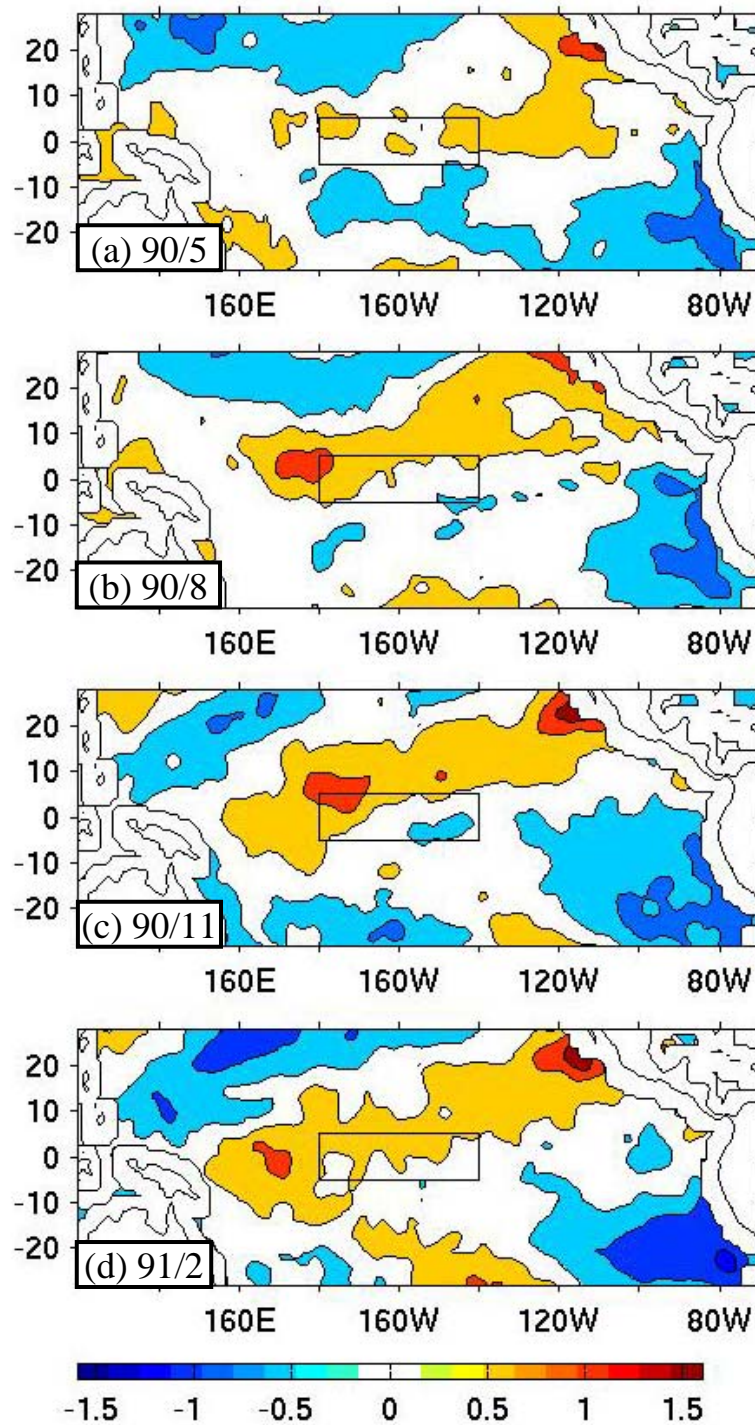


Figure 9. Evolution of SST anomalies in the tropical Pacific from May 1990 to February 1991. The contour intervals are 0.5°C. The “year/month” are indicated in the bottom-left of the panels.

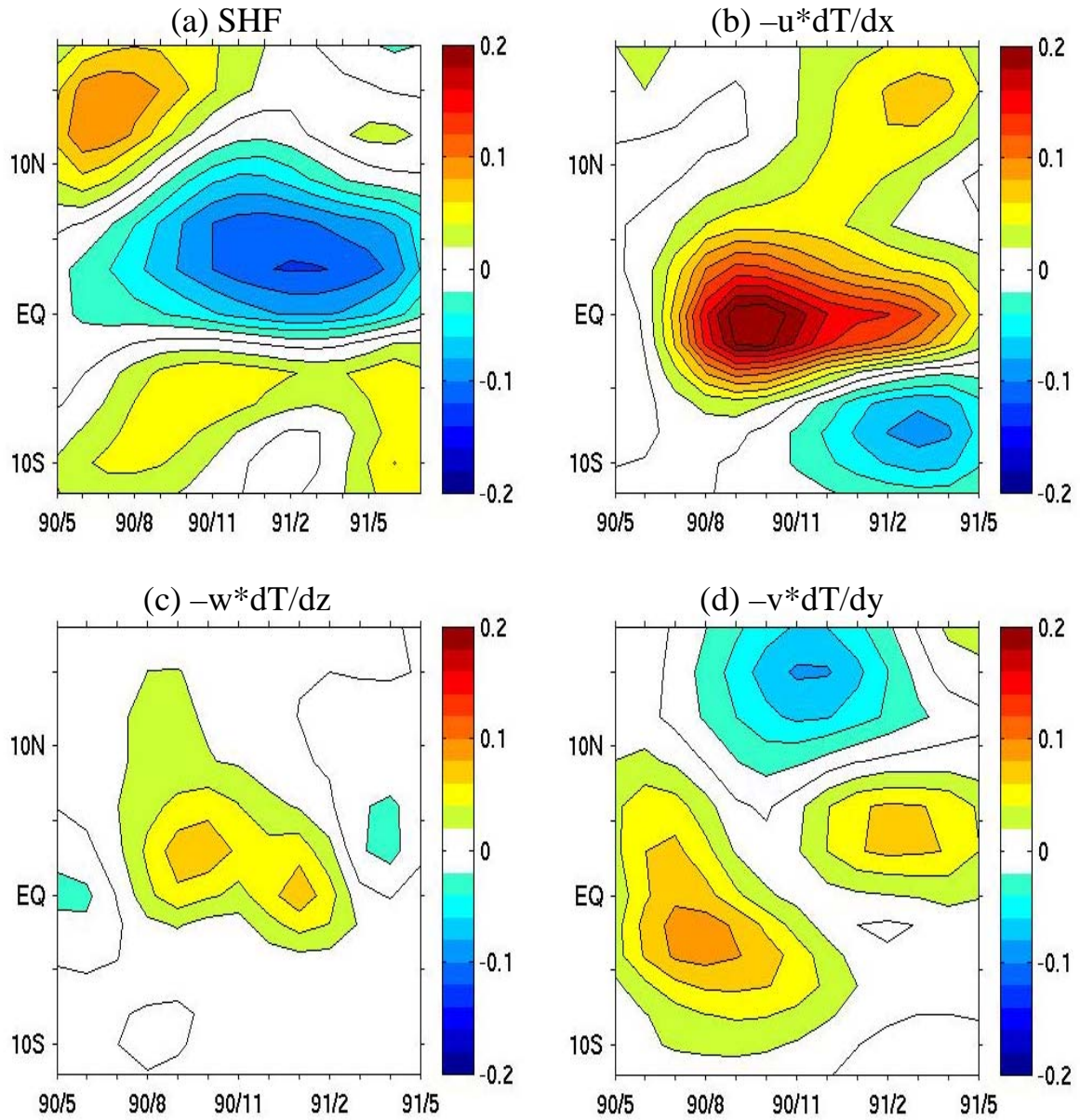


Figure 10. Meridional evolutions of the heat budget terms along the black lines in Fig. 2h for the 1990 event: (a) surface heat flux (SHF) (b)  $-u*dT/dx$  (c)  $-w*dT/dz$  and (d)  $-v*dT/dy$ . The evolutions are shown for the period from May 1990 to May 1991. Contour intervals are 0.02 °C.

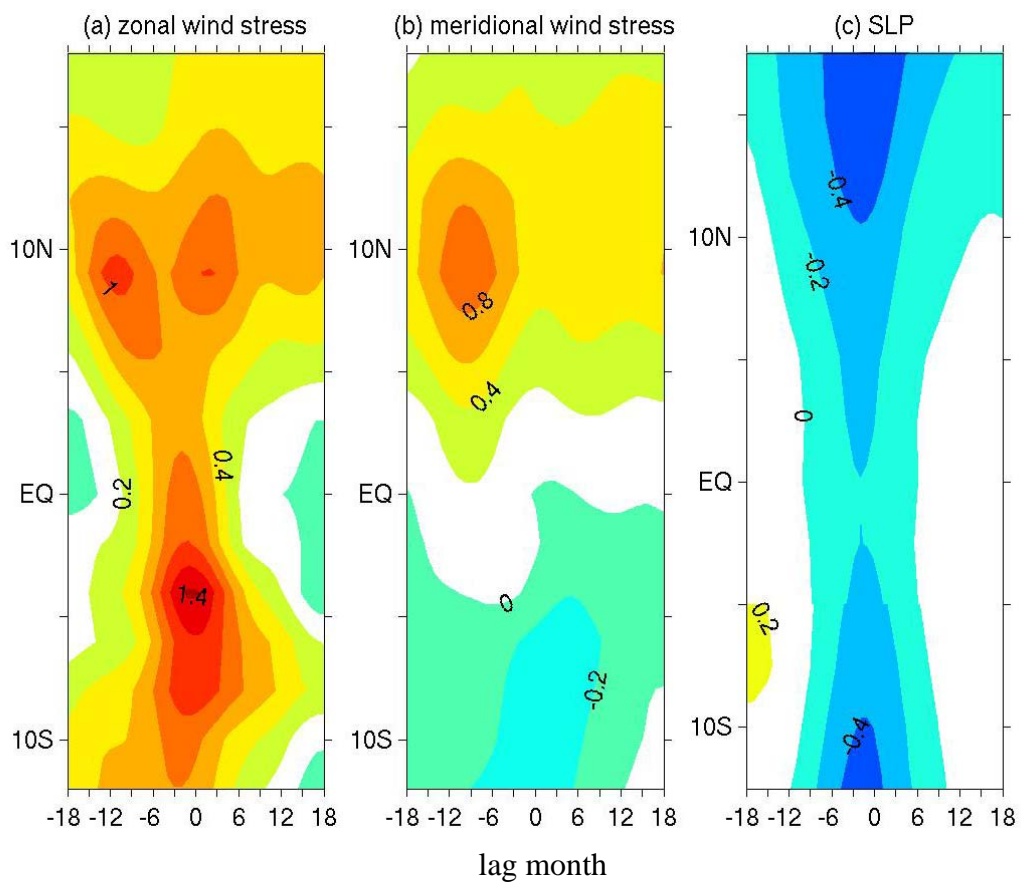


Figure 11. Meridional evolution of Type-2 (a) zonal wind stress (b) meridional wind stress and (c) SLP along the black lines in Fig. 2h. Contour intervals are  $0.2 \text{ cm/s*month*}^\circ\text{C}$  for wind stress and  $0.2 \text{ mb/month*}^\circ\text{C}$  for SLP.

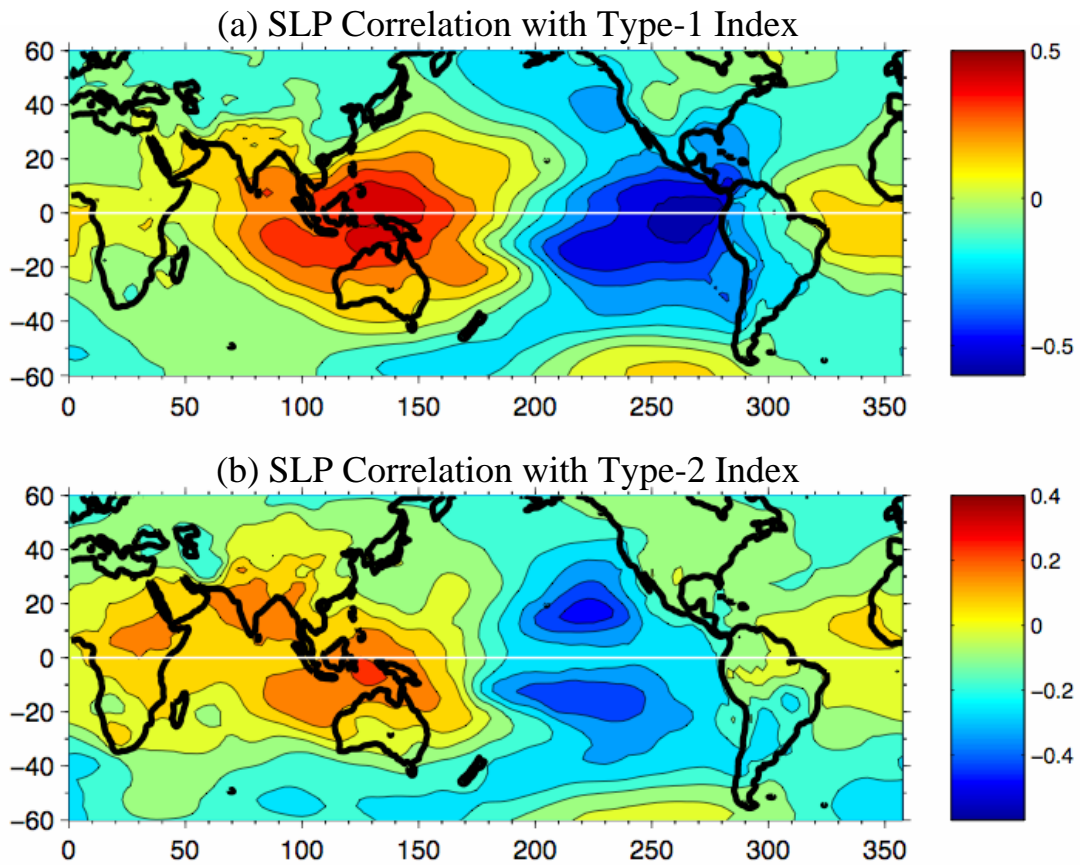


Figure 12. Correlation coefficients of sea level pressure with (a) Type-1 and (b) Type-2 SST indices. The contour interval is 0.1.

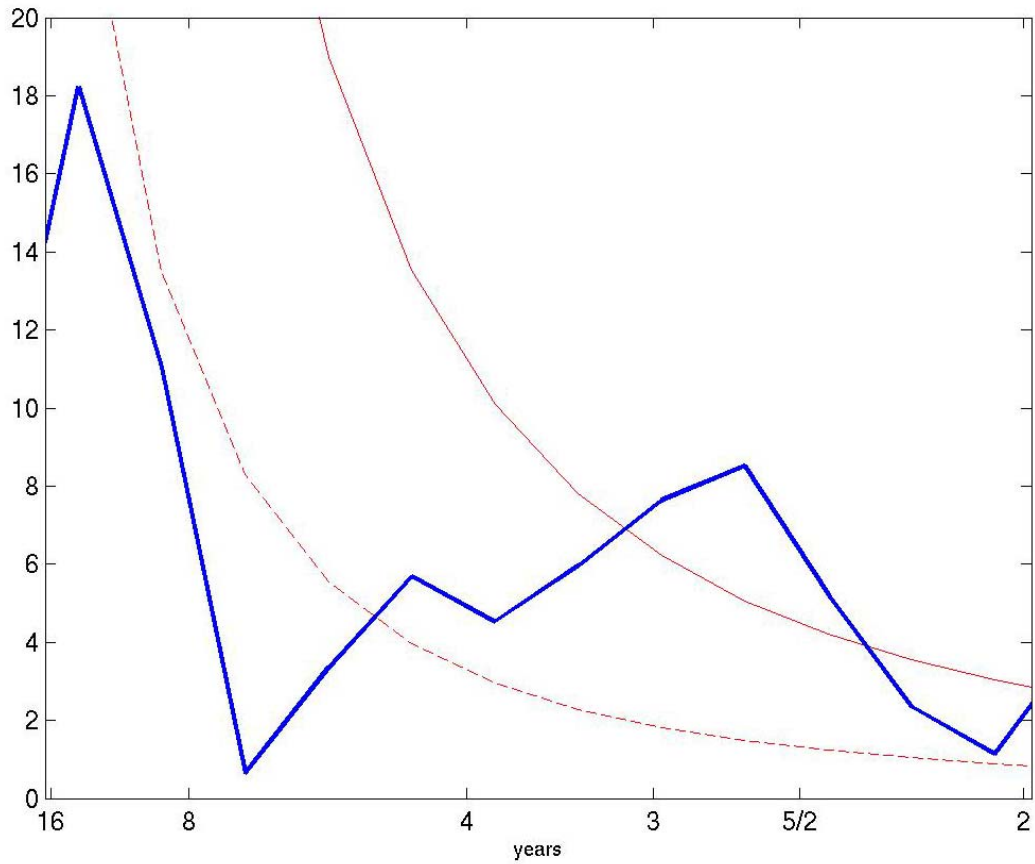


Figure 13. Power spectrum of subtropical high variability calculated from the sea level pressure anomalies averaged in an area between 20°N-40°N and 160°W-110°W. The thin-line denotes the 95% significance level and the dashed-line denotes the red-noise spectrum.

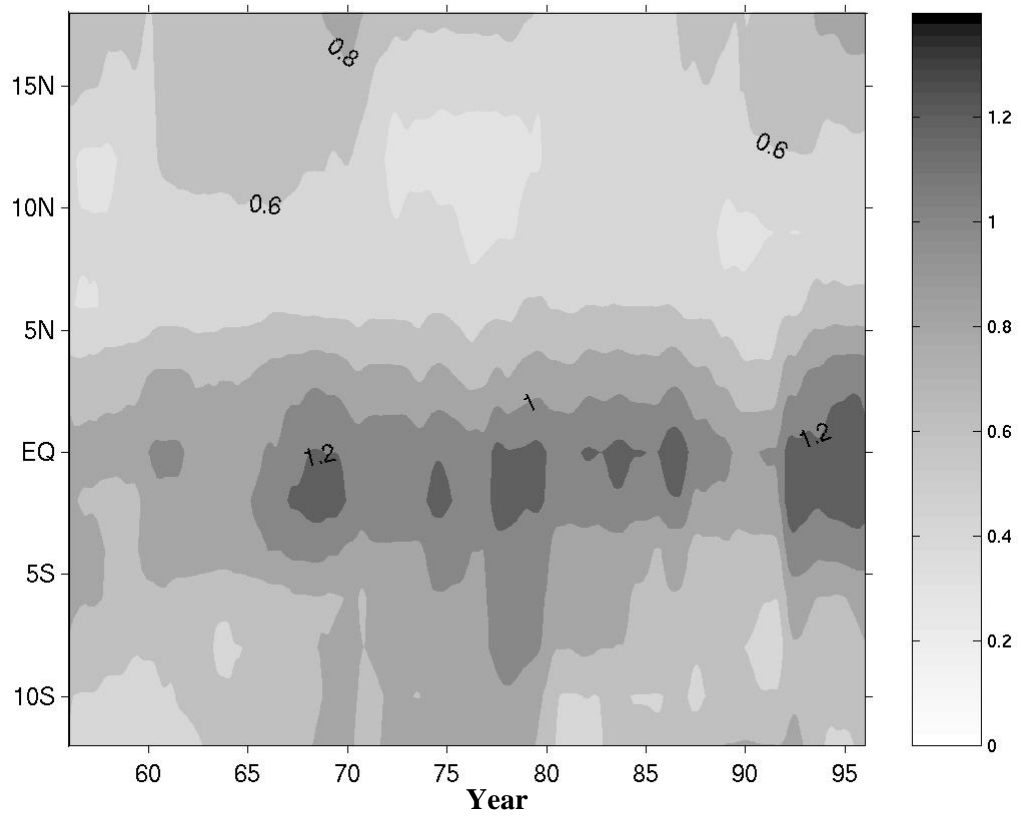


Figure 14. The standard deviations of SST anomalies along the black lines in Fig. 2h from 1958 to 2001 calculated with a 10-year running window. Contour interval is 0.2 °C. The abscissa shows the years.